A Novel Movable UWB Localization System Using UAVs

SUNGTAE MOON[1] AND WONKEUN YOUN [ID]2

[1]School of Computer Engineering, Korea University of Technology and Education, Cheonan-si 31253, Republic of Korea
[2]Department of Autonomous Vehicle System Engineering, Chungnam National University, Yuseong-gu, Daejeon 34134, Republic of Korea

Corresponding author: Wonkeun Youn (wkyoun@cnu.ac.kr)

ABSTRACT Recently, interest in ultrawideband (UWB)-based localization systems has increased in various application fields. However, since UWB anchors are usually fixed, they work only within the limited range that UWB measurement signals can reach. To address this issue, a swarm flight system with movable UWB anchors is developed. One ground station controls multiple unmanned aerial vehicles (UAVs), each of which is equipped with a UWB anchor and real-time kinematic global positioning system (RTK-GPS) capabilities, and collects the precise (centimeter-level) positions of the UWB anchor UAVs through RTK-GPS. In this way, the constraints of existing UWB systems can be alleviated by changing the UWB anchor positions in real time as desired by the user. In addition, this paper proposes a novel localization algorithm using only time-of-flight (TOF) measurements from UWB signals, heading information from an attitude and heading reference system (AHRS), and altitude information from a barometer. The results of UAV flight tests show that the proposed algorithm provides better localization performance than existing algorithms.

INDEX TERMS Interacting multiple model, Kalman filter, localization, swarm flight system, ultrawideband (UWB), unmanned aerial vehicle (UAV).

I. INTRODUCTION

In recent years, quadrotor unmanned aerial vehicles (UAVs) have been frequently used in applications related to the Internet of Things [1] or to supplant human efforts in hazardous environments such as disaster sites [2], [3]. As a result, the problem of accurate and reliable quadrotor localization, as an essential requirement for successful mission performance, has received great attention [4]–[6]. The Global Positioning System (GPS) is one of the most representative technologies for location estimation [7]. Indeed, GPS has been widely used for long-term monitoring in aircraft landing systems [8]. However, the location estimation performance of GPS has been found to be unreliable in some closed and isolated environments, such as urban canyons and indoor spaces [7], [9].

As one possible way to overcome this, radio frequency identification (RFID) technology has been developed to measure distances based on the received signal strength indicator (RSSI) [10]. However, since RFID tags are not precision sensors, the accuracy of RFID-based localization is generally

The associate editor coordinating the review of this manuscript and approving it for publication was Yang Tang [ID].

insufficient. As another alternative, a motion capture system (MCS) is a system that captures objects in space by means of multiple high-speed cameras to obtain their relative positions and poses [11]. When used for positioning, MCSs such as VICON [12] and OptiTrack [13] are accurate to the level of a few millimeters, but their complex layouts and difficult calibration procedures make MCSs difficult to use in some large coverage areas.

To resolve this problem, simultaneous localization and mapping (SLAM) approaches such as oriented FAST and rotated BRIEF (ORB)-SLAM [14], semidirect visual odometry (SVO) [15], and direct sparse odometry (DSO) [16] using image sensors have been actively investigated in recent years. However, the cameras typically used for SLAM rely on rich lighting and environmental textures, whereas most outdoor environments are not textured, which reduces the reliability and accuracy of localization. Additionally, the usability of such image sensors decreases under extreme levels of sunlight due to phenomena such as illuminance variation or fog. In general, camera-based image sensors are greatly affected by the lighting environment. For example, it is difficult to obtain good image data in the dark, and a camera also may not

(a) **National flag of South Korea**

(b) **March 1st, Independence Movement Day**

(c) **Korea Aerospace Research Institute**
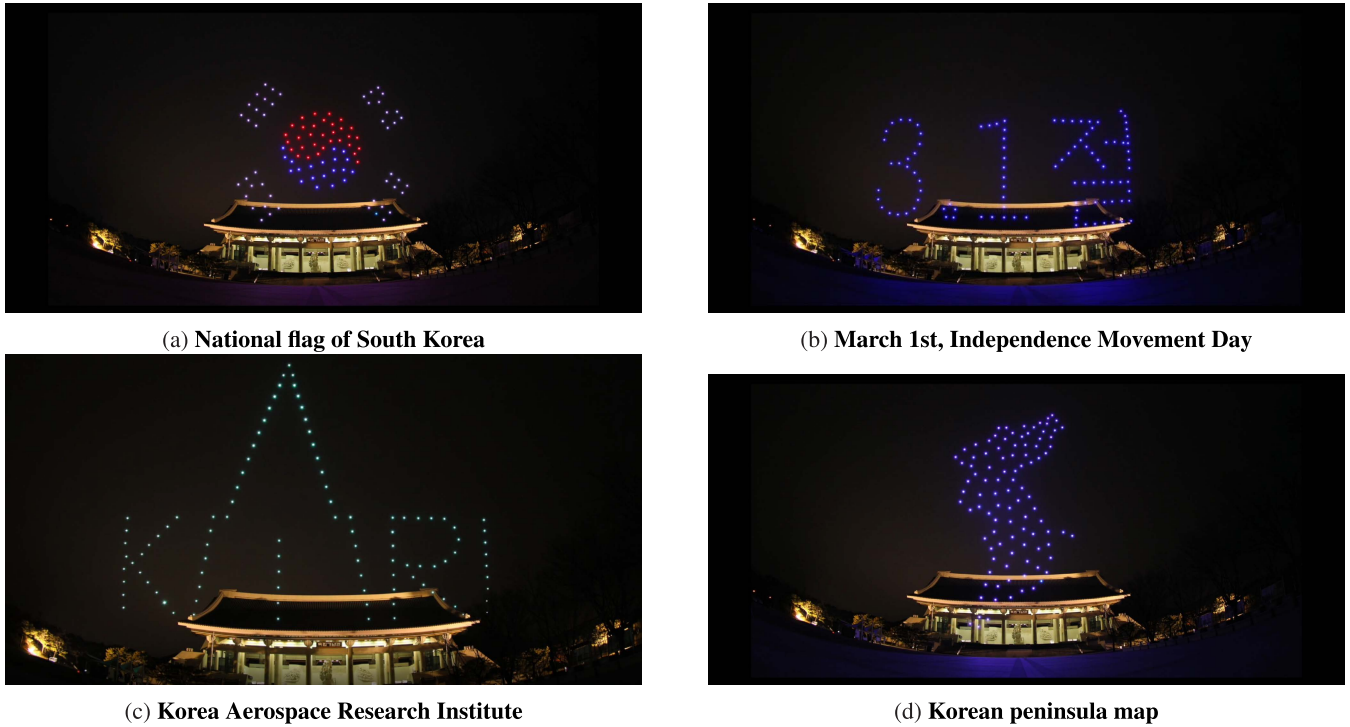

(d) **Korean peninsula map**

FIGURE 1. Examples from a swarm flight demonstration developed by the Korea Aerospace Research Institute.
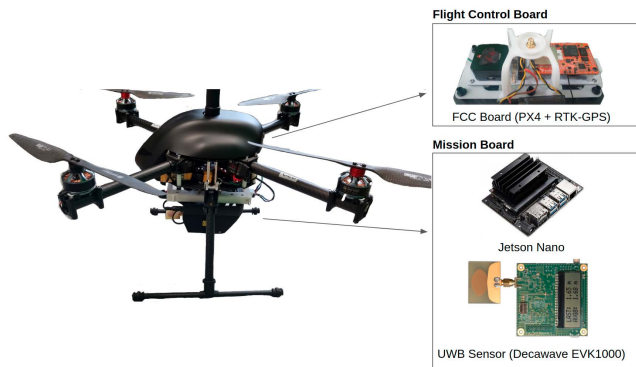

FIGURE 2. Photograph of the UAV system.

work properly if the environment is too bright or if reflected light impinges directly on the camera.

As another approach, recent developments in inexpensive ultrawideband (UWB) transceivers have enabled high-precision time-of-arrival (TOA) or time-of-flight (TOF) measurements in wireless communications [17]. Low-power UWB communication is a communication standard in which wireless impulses can be continuously transmitted and received to achieve precise localization and tracking at a level of several centimeters over a short distance [18]. The frequency band used is 3.1–10.6 GHz, and the operating distance is approximately tens of meters. When UWB communication is utilized as a localization technique, it offers high position resolution because a pulse with a very narrow width is used as a signal. In addition, there is little interference with or influence on existing communication systems because it uses a low transmission power with a low noise level.

In addition, an inertial measurement unit (IMU) is a standard sensor for estimating the state of a UAV, with the advantages of high accuracy, a fast update frequency and a small size [19]. However, an IMU estimates its own position through integration, resulting in continuous error accumulation due to the time-varying bias. Therefore, the fusion of UWB and IMU sensor signals using a Kalman filter is widely used because the UWB contribution limits the integral divergence due to the IMU bias and enables accurate location estimation [20].

However, UWB–IMU sensor fusion faces the following two issues. First, the disadvantage of using UWB technology is that since the UWB measurement range is limited, the UWB coverage area is also limited depending on the locations of the UWB anchors. Specifically, since a UWB anchor is usually fixed, it operates only in a limited range, and the UWB measurement signal will not reach areas beyond that range. Second, since the Kalman-filter-based fusion of UWB and IMU signals involves asynchronous signals, the synchronization process is complicated, and complex parameters for the noise characteristics of the accelerometer and gyroscope are required.

To resolve the above two issues, this paper proposes a system with movable UWB anchors. In the proposed system, a single ground station controls several UAVs, each equipped with a UWB anchor and real-time kinematic (RTK)-GPS capabilities, and collects the precise (centimeter-level) positions of the UWB-anchor-equipped UAVs through RTK-GPS measurements. Thus, the UWB coverage area can be freely adjusted by controlling multiple UAVs equipped with UWB
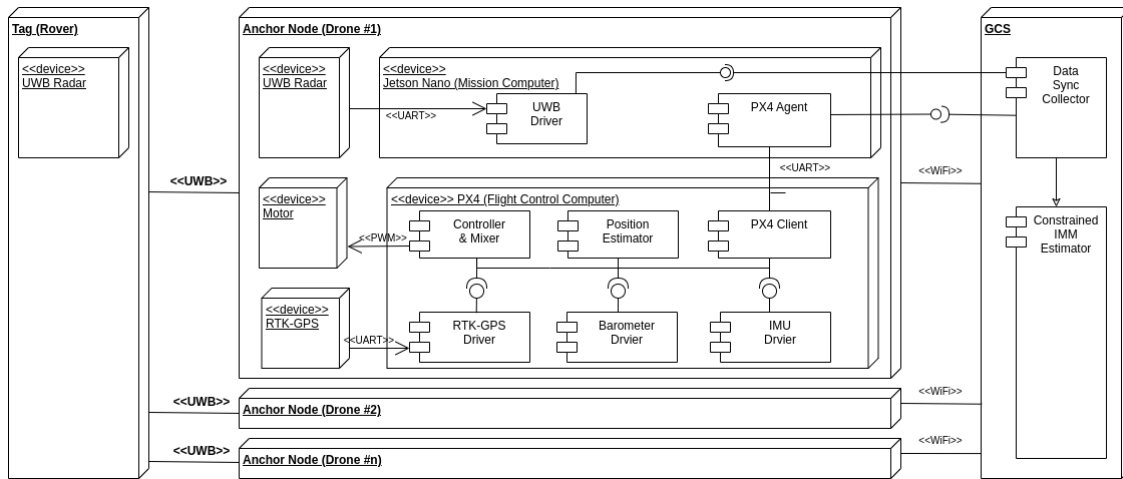
FIGURE 3. Deployment diagram of the proposed movable UWB system.

anchors from the single ground control station (GCS). Additionally, instead of using the acceleration and angular rates from IMUs, we propose an algorithm to improve the UAV location estimation performance by using only the heading information from an attitude and heading reference system (AHRS). This method is much simpler and easier to apply, making it very effective as an independent method that does not depend on a specific UAV model.

In this paper, interacting multiple model (IMM) filtering is applied to accurately estimate the positions of UAVs executing various flight maneuvers. The main contribution of this paper is to propose a novel IMM filtering method that uses heading information from an AHRS and altitude information from a barometer, which results in better localization performance without significantly increasing the computational complexity. The validity of the algorithm has been verified through outdoor flight tests with various trajectories, and a quantitative algorithm performance analysis has been performed.

The rest of the paper is organized as follows. The proposed movable UWB anchor system based on a swarm of UAVs is presented in Section II. As preliminaries, the definitions of the system and measurement models are presented in Section III. The proposed constrained IMM filtering method is summarized in Section IV. Section V briefly describes the experimental setup and results. In Section VI, conclusions are addressed.

II. PROPOSED MOVABLE UWB ANCHOR SYSTEM BASED ON A SWARM OF UAVS

UWB localization systems have been widely used in various applications [21]–[24]. However, the UWB range that can be covered is limited by the locations of the UWB anchors. Since the UWB anchors are usually fixed, they operate only in a limited range, and the UWB measurement signal cannot reach areas beyond that range. In addition, fixed UWB anchors cannot measure the distance to a UWB tag if there are obstacles within the measurement range [25]. That is, existing UWB

localization systems cannot be used for moving tags that are out of range. The proposed movable UWB localization system solves the limited coverage problem by moving the locations of the UWB anchors, which are mounted on UAVs. Therefore, the proposed system can be used to locate objects equipped with UWB tags.

The proposed movable UWB system consists of the movable USB anchor nodes, tag (rover), and GCS subsystem as shown in Fig. 3. The rover uses only a small UWB tag to communicate with the movable UWB anchor node. Thus, in the proposed system, anything with a UWB tag can act as a rover. For the movable UWB anchor nodes, the proposed system utilizes UAVs equipped with RTK-GPS sensors. RTK-GPS sensors can realize position estimation at the centimeter level. RTK-GPS was used only as a ground truth for performance evaluation of the proposed algorithm. The anchor node is divided into the flight control computer and the mission computer

For the flight control computer, a PX4 is used, which is based on open-source software running on the NuttX real-time operating system. When the measurement data received from the barometer and IMU sensor driver are acquired together with the RTK-GPS, the position and attitude are estimated through an estimator based on the extended Kalman filter [7]. Once the position and attitude of the UAV are estimated, the UAV is controlled by adjusting the RPM of the motor through the PWM command in the flight control computer. The PX4 client component transmits the estimation information including sensor data to the mission computer via UART. The mission computer collects data received from UWB sensors and PX4 client components. The PX4 agent transmits the data to the GCS via ROS2 messages. ROS2 is a distributed middleware system running on the Linux operating system.

The GCS is also operated based on ROS2. The data sync collector of GCS receives flight and UWB data from the UWB anchor nodes and synchronizes the anchor data using GPS time information. Once the synchronized data are

received, the position of the target UWB tag is estimated using the proposed constrained IMM estimator.

To develop the proposed movable UWB localization system, we update the swarm flight system by adding a mission board, including a mission computer and UWB sensors, as shown in Fig. 2. The UAV platform is designed to replace the currently employed mission board and uses a general quad-copter frame equipped with an open-source PX4 system [27], an IMU (an LSM303D integrated accelerometer/magnetometer and L3GD20 gyroscope), a barometer (MS5611, TE Connectivity), and an RTK-GPS receiver (Piksi, Swift Navigation). The mission board includes an NVIDIA Jetson nano computer to run the Robot Operating System version 2 (ROS2) and the UWB sensors (EVK-1000, Decawave).

The proposed system can control multiple UAVs simultaneously to find the location of a UWB tag. Recently, the Korea Aerospace Research Institute (KARI) developed a swarming flight system that can operate with an arbitrary number of UAVs [26]. This system was used in a drone show in which multiple UAVs were precisely controlled using RTK-GPS, as shown in Fig. 1. For a detailed flight video, please visit the following URL: https://www.youtube.com/watch?v=TgCKhgIjWW8.

III. PRELIMINARY DEFINITIONS
A. CONSTANT VELOCITY MODEL
The constant velocity (CV) model is defined as follows [28]:

$$\mathbf{x}_{k+1} = \begin{bmatrix} 1 & 0 & 0 & T_s & 0 & 0 \\ 0 & 1 & 0 & 0 & T_s & 0 \\ 0 & 0 & 1 & 0 & 0 & T_s \\ 0 & 0 & 0 & 1 & 0 & 0 \\ 0 & 0 & 0 & 0 & 1 & 0 \\ 0 & 0 & 0 & 0 & 0 & 1 \end{bmatrix} \mathbf{x}_k$$

TABLE 1. Specifications of the UAV system.

Parameter	UAV specification
Weight	2.706 Kg
Payload	2 kg
Flight time	20 min
Dimension	650 mm
Propeller	13 inch

$$+ \begin{bmatrix} \frac{1}{2}T_s^2 & 0 & 0 \\ 0 & \frac{1}{2}T_s^2 & 0 \\ 0 & 0 & \frac{1}{2}T_s^2 \\ T_s & 0 & 0 \\ 0 & T_s & 0 \\ 0 & 0 & T_s \end{bmatrix} w_{k,\text{CV}} \quad (1)$$

where T_s denotes the sampling time interval and the state of the UAV is defined as $\mathbf{x}_k = [x_k \ y_k \ z_k \ \dot{x}_k \ \dot{y}_k \ \dot{z}_k]^T$. The first three state variables (x_k, y_k, z_k) are the x, y, and z positions, and the last three state variables ($\dot{x}_k$, $\dot{y}_k$, $\dot{z}_k$) are the x, y, and z velocities. $w_{k,\text{CV}}$ is a zero-mean Gaussian white noise term with a covariance matrix $Q_{k,\text{CV}}$ to cover unexpected acceleration.

B. COORDINATED TURN MODEL
The state of the target in the coordinated turn (CT) model is defined as $\mathbf{x}_k = [x_k \ y_k \ z_k \ \dot{x}_k \ \dot{y}_k \ \dot{z}_k \ \Omega_k]^T$, including the turning rate Ω_k. The CT model is expressed as (2), shown at the bottom of the page [29], where $w_{k,\text{CT}}$ is zero-mean Gaussian white noise with covariance matrix $Q_{k,\text{CT}}$.

C. UWB MEASUREMENT MODEL
The range of the measurements $z_k^{(l)}$ ($l = 1, \ldots, m$), where m denotes the number of UWB measurements, can

$$\mathbf{x}_{k+1} = \begin{bmatrix} 1 & 0 & 0 & \frac{\sin \Omega_k T_s}{\Omega_k} & \frac{\cos \Omega_k T_s - 1}{\Omega_k} & 0 & 0 \\ 0 & 1 & 0 & \frac{1 - \cos \Omega_k T_s}{\Omega_k} & \frac{\sin \Omega_k T_s}{\Omega_k} & 0 & 0 \\ 0 & 0 & 1 & 0 & 0 & 1 & 0 \\ 0 & 0 & 0 & \cos \Omega_k T_s & -\sin \Omega_k T_s & 0 & 0 \\ 0 & 0 & 0 & \sin \Omega_k T_s & \cos \Omega_k T_s & 0 & 0 \\ 0 & 0 & 0 & 0 & 0 & 1 & 0 \\ 0 & 0 & 0 & 0 & 0 & 0 & 1 \end{bmatrix} \mathbf{x}_k$$

$$+ \begin{bmatrix} \frac{1}{2}T_s^2 & 0 & 0 \\ 0 & \frac{1}{2}T_s^2 & 0 \\ 0 & 0 & \frac{1}{2}T_s^2 \\ T_s & 0 & 0 \\ 0 & T_s & 0 \\ 0 & 0 & T_s \end{bmatrix} w_{k,\text{CT}} \quad (2)$$

be expressed as follows [30]:

$$
\mathbf{z}_k = \begin{bmatrix} z_k^{(1)} \\ \vdots \\ z_k^{(m)} \end{bmatrix}
$$

$$
= \begin{bmatrix} \sqrt{(x_k - x_{1,k})^2 + (y_k - y_{1,k})^2 + (z_k - z_{1,k})^2} \\ \vdots \\ \sqrt{(x_k - x_{m,k})^2 + (y_k - y_{m,k})^2 + (z_k - z_{m,k})^2} \end{bmatrix} \tag{3}
$$

$$
+ \begin{bmatrix} v_k^{(1)} \\ \vdots \\ v_k^{(m)} \end{bmatrix} \tag{4}
$$

where x_k and y_k denote the x and y positions, respectively, of the target UWB tag at time index k; $x_{m,k}$ and $y_{m,k}$ similarly denote the x and y positions of the m-th UWB anchor; and $v_k^{(m)}$ is the measurement noise of the m-th UWB anchor.

D. MULTILATERATION

To estimate the initial position of the UWB tag based on UWB TOF range measurements, the algorithm of [31] is adopted. Based on a linear algebraic method, this algorithm has low computational complexity and can be applied in wireless UWB sensor networks for real-time applications.

Rearranging (3) yields [31]

$$
\begin{bmatrix} 1 & -2x_{1,k} & -2y_{1,k} & -2z_{1,k} \\ 1 & -2x_{2,k} & -2y_{2,k} & -2z_{2,k} \\ 1 & -2x_{3,k} & -2y_{3,k} & -2z_{3,k} \\ \vdots & \vdots & \vdots & \vdots \\ 1 & -2x_{m,k} & -2y_{m,k} & -2z_{m,k} \end{bmatrix} \begin{bmatrix} x_k^2 + y_k^2 + z_k^2 \\ x_k \\ y_k \\ z_k \end{bmatrix}
$$

$$
= \begin{bmatrix} z_k^{(1)} - (x_{1,k}^2 + y_{1,k}^2 + z_{1,k}^2) \\ z_k^{(2)} - (x_{2,k}^2 + y_{2,k}^2 + z_{2,k}^2) \\ z_k^{(3)} - (x_{3,k}^2 + y_{3,k}^2 + z_{3,k}^2) \\ \vdots \\ z_k^{(m)} - (x_{3,k}^m + y_{3,k}^m + z_{3,k}^m) \end{bmatrix} \tag{5}
$$

Equation (5) can be represented in matrix form as follows:

$$
\mathbf{A}\mathbf{x} = \mathbf{b} \tag{6}
$$

The solution $\hat{\mathbf{x}}$ of (6) can be computed using the weighted least squares method if the UWB range measurements are uncorrelated and have different uncertainties, as follows:

$$
\hat{\mathbf{x}} = (\mathbf{A}^\mathbf{T}\mathbf{W}^{-1}\mathbf{A})^{-1}\mathbf{A}^\mathbf{T}\mathbf{W}^{-1}\mathbf{b} \tag{7}
$$

where $\mathbf{W}$ denotes the covariance matrix of the random errors for the range measurements provided by the UWB sensors. Here, a recursive weighted least squares algorithm is implemented following [31].

IV. PROPOSED CONSTRAINED IMM FILTERING METHOD

The nonlinear system model $\mathbf{f}^j(\cdot)$ of the j-th UAV mode and the corresponding UWB measurement model $\mathbf{h}^j(\cdot)$ are as follows [28]:

$$
\mathbf{x}_{k+1}^j = \mathbf{f}^j(\mathbf{x}_k^j) + \mathbf{w}_k^j \tag{8}
$$

$$
\mathbf{z}_k^j = \mathbf{h}^j(\mathbf{x}_k^j) + \boldsymbol{v}_k^j \tag{9}
$$

where $\mathbf{x}_k^j \in \mathbb{R}^n$ and $\mathbf{z}_k^j \in \mathbb{R}^m$ are the state vector and measurement vector, respectively, at time index k. The process noise $\mathbf{w}_k^j$ and measurement noise $\boldsymbol{v}_k^j$ are uncorrelated white Gaussian noise with zero mean, as follows:

$$
E\left[\mathbf{w}_k^j \mathbf{w}_l^{jT}\right] = \mathbf{Q}_k \delta_{kl}, \quad E\left[\boldsymbol{v}_k^j \boldsymbol{v}_l^{jT}\right] = \mathbf{R}_k \delta_{kl}
$$

$$
E\left[\mathbf{w}_k^j \boldsymbol{v}_l^{jT}\right] = 0 \tag{10}
$$

The mode transition probability (MTP) from the i-th mode to the j-th mode at consecutive times (e.g., $k-1$ to k) can be defined as

$$
p_{ij} = P\{M_k = j | M_{k-1} = i\} \tag{11}
$$

where N_r is set to 2 in this paper. The IMM filtering method consists of the following four procedures, applied in a recursive manner.

A. INTERACTION/MIXING PROCEDURE

The mixing probability $\mu_{k-1|k-1}^{ij}$ between modes M_i and M_j at consecutive times (e.g., $k-1$ to k) can be computed utilizing p_{ij}, as follows [29]:

$$
\mu_{k-1|k-1}^{ij} = \frac{1}{\bar{c}_j} p_{ij} \mu_{k-1}^i \tag{12}
$$

where $\bar{c}_j = \sum_{i=1}^{N_r} p_{ij} \mu_{k-1}^i$.

The mixed state $\hat{\mathbf{x}}_{k-1|k-1}^{0j}$ and the corresponding covariance $\mathbf{P}_{k-1|k-1}^{0j}$ of each subfilter model can be obtained from the previous estimate $\hat{\mathbf{x}}_{k-1|k-1}^i$ as follows:

$$
\hat{\mathbf{x}}_{k-1|k-1}^{0j} = \sum_{i=1}^{N_r} \mu_{k-1|k-1}^{ij} \hat{\mathbf{x}}_{k-1|k-1}^i
$$

$$
\mathbf{P}_{k-1|k-1}^{0j} = \sum_{i=1}^{N_r} \mu_{k-1|k-1}^{ij}
$$
$$
\cdot \left(\begin{array}{c} \mathbf{P}_{k-1|k-1}^i + [\hat{\mathbf{x}}_{k-1|k-1}^i - \hat{\mathbf{x}}_{k-1|k-1}^{0j}] \\ \cdot [\hat{\mathbf{x}}_{k-1|k-1}^i - \hat{\mathbf{x}}_{k-1|k-1}^{0j}]^T \end{array} \right) \tag{13}
$$

B. MODE-CONDITION FILTERING PROCEDURE

To compute the predicted state $\hat{\mathbf{x}}_{k|k-1}^j$ and the covariance $\mathbf{P}_{k|k-1}^j$ of the j-th subfilter, the standard extended Kalman filter (EKF) is implemented as follows:

$$
\hat{\mathbf{x}}_{k|k-1}^j = \mathbf{f}^j(\hat{\mathbf{x}}_{k-1|k-1}^{0j})
$$

$$\mathbf{P}_{k|k-1}^j = \mathbf{F}_{k-1}^j \mathbf{P}_{k-1|k-1}^{0j} \left(\mathbf{F}_{k-1}^j\right)^T + \Gamma_{k-1}^j \mathbf{Q}_{k-1}^j \left(\Gamma_{k-1}^j\right)^T \tag{14}$$

where the Jacobian matrix for the system dynamic equation, $\mathbf{F}_{k-1}^j$, is defined as

$$\mathbf{F}_{k-1}^j = \left.\frac{\partial \mathbf{f}^j}{\partial x}\right|_{x=\hat{\mathbf{x}}_{k-1|k-1}^{0j}}$$

The updated state $\hat{\mathbf{x}}_{k|k}^j$ and the corresponding error covariance $\mathbf{P}_{k|k}^j$ are computed as

$$\hat{\mathbf{x}}_{k|k}^j = \hat{\mathbf{x}}_{k|k-1}^j + \mathbf{K}_k^j \boldsymbol{v}_k^j$$
$$\mathbf{P}_{k|k}^j = \mathbf{P}_{k|k-1}^j - \mathbf{K}_k^j \mathbf{S}_k^j \left(\mathbf{K}_k^j\right)^T \tag{15}$$

where the Kalman gain $\mathbf{K}_k^j$ and the innovation $\boldsymbol{v}_k^j$ are defined as

$$\mathbf{K}_k^j = \mathbf{P}_{k|k-1}^j \left(\mathbf{H}_k^j\right)^T \left(\mathbf{S}_k^j\right)^{-1} \tag{16}$$
$$\boldsymbol{v}_k^j = \mathbf{z}_k - \mathbf{h}^j(\hat{\mathbf{x}}_{k|k-1}^j) \tag{17}$$

and $\mathbf{S}_k^j$ can be expressed as

$$\mathbf{S}_k^j = \mathbf{H}_k^j \mathbf{P}_{k|k-1}^j \left(\mathbf{H}_k^j\right)^T + \mathbf{R}_k^j \tag{18}$$

where $\mathbf{H}_k^j$ is defined as

$$\mathbf{H}_k^j = \left.\frac{\partial \mathbf{h}^j}{\partial x}\right|_{x=\hat{\mathbf{x}}_{k|k-1}^j}$$

C. MODE PROBABILITY UPDATE PROCEDURE

The mode probability μ_k^i is defined as

$$\mu_k^i = \frac{1}{c} \Lambda_{i,k} \bar{c}_i, \quad i = 1, \cdots, N_r \tag{19}$$

where

$$c = \sum_{i=1}^{N_r} \Lambda_{i,k} \bar{c}_i \tag{20}$$

and $\Lambda_{i,k}$ is a likelihood function given by

$$\Lambda_{i,k} = \frac{1}{\sqrt{\left|2\pi \mathbf{S}_k^j\right|}} \exp\left(-\frac{1}{2}\left(\boldsymbol{v}_k^i\right)^T \left(\mathbf{S}_k^j\right)^{-1} \boldsymbol{v}_k^i\right) \tag{21}$$

D. ESTIMATE AND COVARIANCE COMBINATION PROCEDURE

The state and covariance in the IMM algorithm can be defined as

$$\hat{\mathbf{x}}_{k|k} = \sum_{i=1}^{N_r} \mu_k^i \hat{\mathbf{x}}_{k|k}^i$$

$$\mathbf{P}_{k|k} = \sum_{i=1}^{N_r} \mu_k^i \left(\mathbf{P}_{k|k}^i + [\hat{\mathbf{x}}_{k|k}^i - \hat{\mathbf{x}}_{k|k}] \cdot [\hat{\mathbf{x}}_{k|k}^i - \hat{\mathbf{x}}_{k|k}]^T\right) \tag{22}$$

E. CONSTRAINED FILTERING

The principle of the Kalman filter is to maximize the probability density function (pdf) $pdf(\mathbf{x}_k|\mathbf{Z}_k)$, which can be expressed as

$$\hat{\mathbf{x}}_k = argmax_{\mathbf{x}_k} pdf(\mathbf{x}_k|\mathbf{Z}_k) \tag{23}$$

where $\hat{\mathbf{x}}_k$ denotes the solution of the Kalman filter that maximizes $pdf(\hat{\mathbf{x}}_k|\mathbf{Z}_k)$. Under the assumption of a Gaussian distribution, $pdf(\hat{\mathbf{x}}_k|\mathbf{Z}_k)$ can be expressed as

$$pdf(\mathbf{x}_k|\mathbf{Z}_k) = \frac{\exp\left(-\frac{1}{2}(\mathbf{x}_k - \bar{\mathbf{x}}_k)^T \mathbf{P}_k^{-1}(\mathbf{x}_k - \bar{\mathbf{x}}_k)\right)}{(2\pi)^{n/2} |\mathbf{P}_k|^{1/2}} \tag{24}$$

Maximizing (24) is equivalent to maximizing *ln pdf* $(\mathbf{x}_k|\mathbf{Z}_k)$, which means minimizing $(\mathbf{x}_k - \bar{\mathbf{x}}_k)^T \mathbf{P}_k^{-1}(\mathbf{x}_k - \bar{\mathbf{x}}_k)$. If we have an additional constraint such that $\mathbf{D}\mathbf{x}_k = d$, then the solution to this constrained optimization problem is the constrained state estimate $\tilde{\mathbf{x}}_k$, which can be defined as

$$\tilde{\mathbf{x}}_k = argmax_{\mathbf{x}_k} (\mathbf{x}_k - \bar{\mathbf{x}}_k)^T \mathbf{P}_k^{-1}(\mathbf{x}_k - \bar{\mathbf{x}}_k)$$
$$such that \mathbf{D}\tilde{\mathbf{x}}_k = d \tag{25}$$

The solution to (25) can be computed by using the Lagrange multiplier approach as follows:

$$\mathbf{L} = (\mathbf{x}_k - \bar{\mathbf{x}}_k)^T \mathbf{P}_k^{-1}(\mathbf{x}_k - \bar{\mathbf{x}}_k) + 2\lambda^T \left(\mathbf{D}\tilde{\mathbf{x}}_k - d\right)$$
$$\frac{\partial \mathbf{L}}{\partial \tilde{\mathbf{x}}_k} = \mathbf{P}_k^{-1}\left(\tilde{\mathbf{x}}_k - \bar{\mathbf{x}}_k\right) + \mathbf{D}^T \lambda = 0$$
$$\frac{\partial \mathbf{L}}{\partial \lambda} = \mathbf{D}\tilde{\mathbf{x}}_k - d = 0 \tag{26}$$

where λ denotes the *n*-th dimensional Lagrange multiplier. The solution to (26) can be obtained as

$$\lambda = \left(\mathbf{D}\mathbf{P}_k\mathbf{D}^T\right)^{-1} \left(\mathbf{D}\hat{\mathbf{x}}_k - d\right)$$
$$\tilde{\mathbf{x}}_k = \hat{\mathbf{x}}_k + \mathbf{P}_k\mathbf{D}^T \left(\mathbf{D}\mathbf{P}_k\mathbf{D}^T\right)^{-1} \left(\mathbf{D}\hat{\mathbf{x}}_k - d\right) \tag{27}$$

It can be deduced from (27) that the constrained state estimate $\tilde{\mathbf{x}}_k$ is equivalent to the unconstrained state estimate $\hat{\mathbf{x}}_k$, which is the a posteriori estimate after the measurement update, minus a correction term.

Typically, to allow a UAV to fly autonomously, the UAV is equipped with an AHRS that provides attitude information, including roll, pitch and yaw. If the yaw or heading (i.e., ψ_k) is available from the AHRS, then the following equation can be obtained:

$$tan\psi_k = x_k/y_k = \mathbf{x}_k(1)/\mathbf{x}_k(2)$$
$$= \dot{x}_k/\dot{y}_k = \mathbf{x}_k(4)/\mathbf{x}_k(5) \tag{28}$$

The constraints that relate to the horizontal positions (i.e., x_k and y_k) and velocities (i.e., $\dot{x}_k$ and $\dot{y}_k$) can be re-expressed in matrix form as follows:

$$\mathbf{D}_k\mathbf{x}_k = d_k \tag{29}$$

where

$$\mathbf{D}_k = \begin{bmatrix} 1 & -tan\psi_k & 0 & 0 & 0 & 0 & 0 \\ 0 & 0 & 0 & 1 & -tan\psi_k & 0 & 0 \end{bmatrix} \tag{30}$$
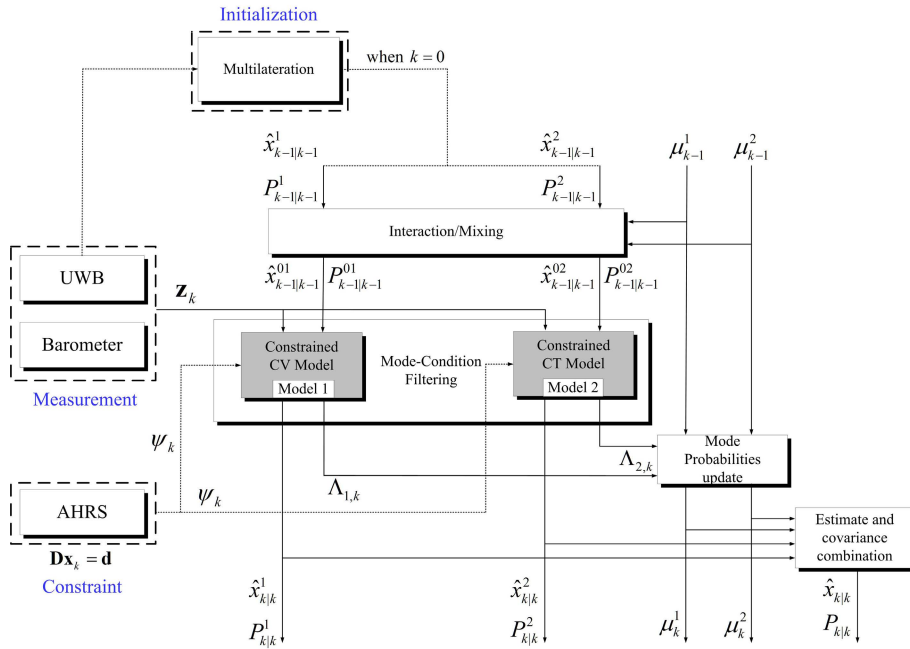
FIGURE 4. Schematic of the proposed constrained IMM filtering method using heading-aided UWB measurements with barometer information.

Algorithm 1 The Proposed Constrained IMM Algorithm

Inputs: $\mathbf{f}_k^j(\cdot)$, $\mathbf{h}_k^j(\cdot)$, $\mathbf{H}_k^j$, $\mathbf{z}_k$, $\hat{\mathbf{x}}_{k-1|k-1}^j$, $\mathbf{P}_{k-1|k-1}^j$, μ_0, p_{ij}, n, m, N_r

1) Initialization:
    1. Calculate the initial location $\hat{\mathbf{x}}_0^j(1:3)$ for $j = 1$
       and 2 using (6)

2) Interaction/Mixing:
    1. Calculate μ_{k-1}^{ij} using (12)
    2. Calculate $\hat{\mathbf{x}}_{k-1|k-1}^{0j}$ and $\mathbf{P}_{k-1|k-1}^{0j}$ using (13)

3) Subfilter Model Filtering:

for $j = 1 : N_r$ ▷ N_r: number of modes
  Predict:
    3. Calculate $\hat{\mathbf{x}}_{k|k-1}^j$ and $\mathbf{P}_{k|k-1}^j$ using (14)
  Update:
    4. Calculate $\hat{\mathbf{x}}_{k|k}^j$ and $\mathbf{P}_{k|k}^j$ using (15)
    5. Calculate $\tilde{\mathbf{x}}_k$ using (31)

4) Mode Probability Update:
    6. Calculate μ_k^i using (19)

Subfilter Model Outputs: $\hat{\mathbf{x}}_{k|k}^j$, $\mathbf{P}_{k|k}^j$

5) Combination:
    7. Calculate $\hat{\mathbf{x}}_{k|k}$ and $\mathbf{P}_{k|k}$ using (22)

Outputs: $\tilde{\mathbf{x}}_k$, $\mathbf{P}_{k|k}$

Then, the constrained estimate $\tilde{\mathbf{x}}_k$ can be computed from the a posteriori estimate as follows:

$$\tilde{\mathbf{x}}_k = \hat{\mathbf{x}}_{k|k} + \mathbf{P}_k \mathbf{D}_k^T \left(\mathbf{D}_k \mathbf{P}_k \mathbf{D}_k^T \right)^{-1} \left(\mathbf{D}_k \hat{\mathbf{x}}_{k|k} - d_k \right) \quad (31)$$

The proposed algorithm is summarized in Algorithm 1 and Fig. 4. The initial position of the UAV is calculated through the multilateration method, as described in Section III.D, and
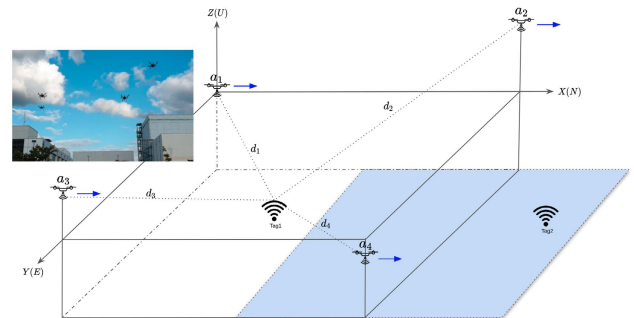

FIGURE 5. Test environment.

is used as the initial position estimate for the subsequent IMM filter. In the IMM filter, two models (the CV model and the CT model) run in parallel, and the UWB range measurement and the altitude value from the barometer are used as measurement values for each subfilter. Then, the proposed algorithm constructs a constraint condition based on the heading value from the AHRS and updates the state values in accordance with (27).

V. EXPERIMENTS AND DISCUSSION

A. FLIGHT EXPERIMENTAL ENVIRONMENT

To evaluate the effectiveness of the proposed algorithm, a total of four UWB anchor nodes were used to estimate the location of a UWB tag. Four UAVs equipped with UWB anchors were used as UWB anchor nodes to widen the coverage of the UWB signals, and this approach permitted better estimation of the target drone's altitude, as the UWB anchors could be placed at different heights as desired. Specifically, a UAV equipped with UWB was used as the target tag. For the
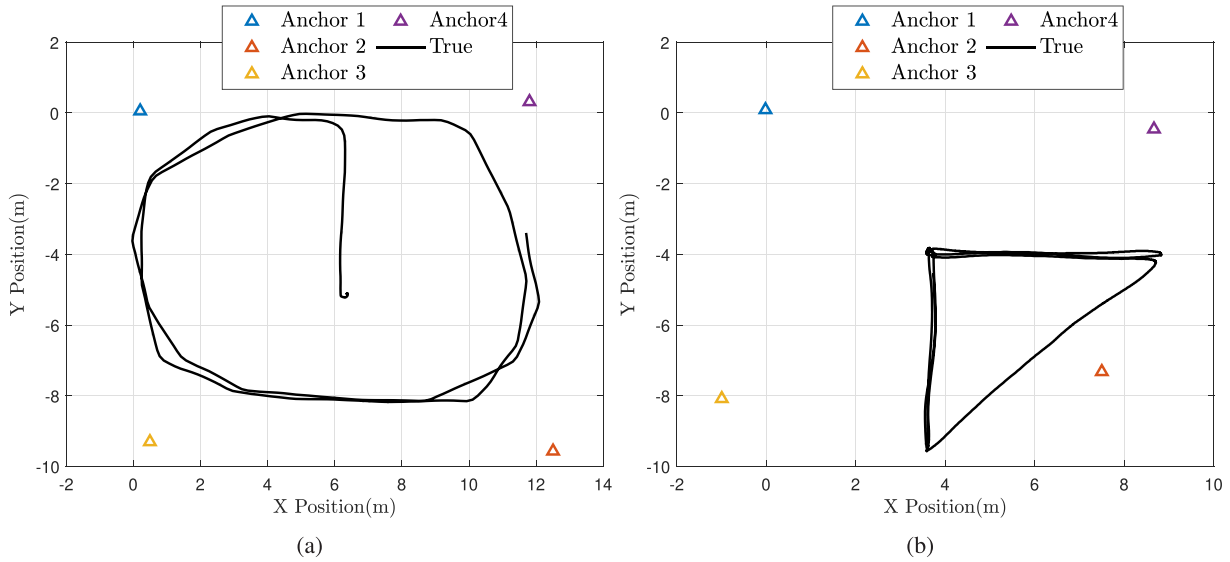
FIGURE 6. UAV trajectories during (a) circular and (b) triangular motions.
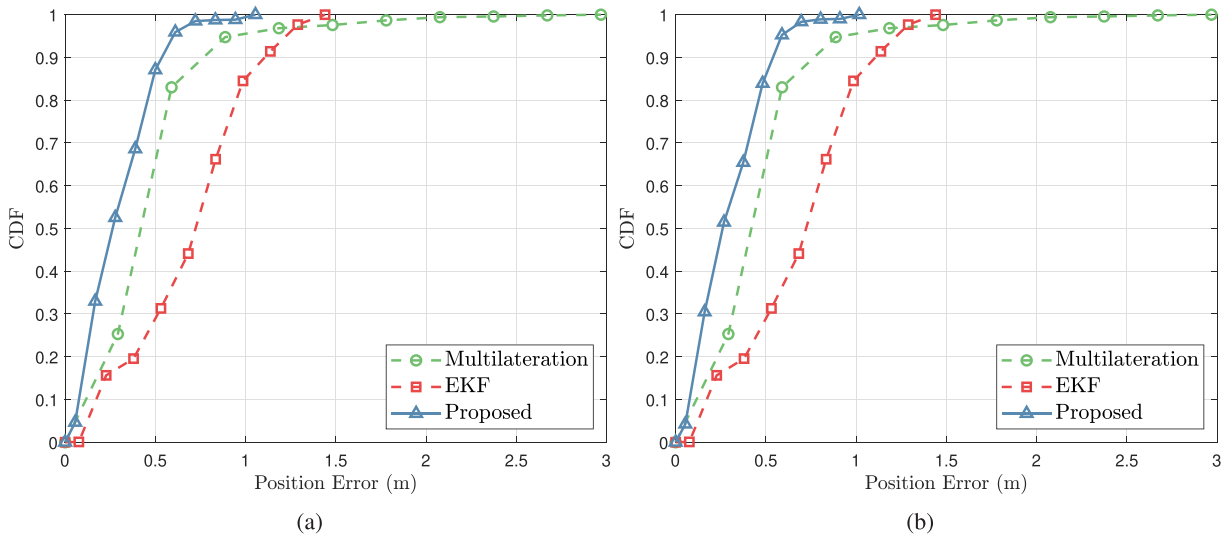

FIGURE 7. CDFs of multilateration, the EKF, and the proposed algorithm during (a) circular and (b) triangular motions.

experiment, as shown in Fig. 5, the four UAVs equipped with UWB anchors were moved to the desired UWB anchor node locations and hovered at approximately 5 m $\pm$ 2 m, while the UAV equipped with the target UWB tag flew within the measurable range of the UWB anchor nodes.

For accurate performance evaluation, flight tests were performed with two flight trajectories, circular and triangular, as shown in Fig. 6. As shown in this figure, the UWB flight tests were performed within the range that the UWB anchor nodes could measure. In the figure, the true value is a value measured with RTK-GPS technology, which is used as the ground-truth value for the subsequent quantitative performance evaluation.

Flight data were stored for approximately 390 and 120 seconds for the triangular and circular motions, respectively, and the sampling interval T_s was 0.1s. The approximate average velocity of the UAV was 2m/s. In these

experiments, $\mathbf{Q}_k$ was set to diag([1, 1, 1, 0.5, 0.5, 0.5]) and diag([1, 1, 1, 0.5, 0.5, 0.5, 1]) for the CV and CT models, respectively, and $\mathbf{R}_k$ was set to $0.45 \cdot I_4$, where I_4 denotes the 4×4 identity matrix. The initial mode probabilities and MTP of the proposed constrained IMM filter were set to

$$ \mu_0 = \begin{bmatrix} 0.85 & 0.15 \end{bmatrix}, \quad p_{ij} = \begin{bmatrix} 0.8 & 0.2 \\ 0.2 & 0.8 \end{bmatrix}. $$

B. EXPERIMENTAL ANALYSIS

To investigate its superiority, the proposed algorithm was compared with the multilateration [31] and EKF approaches using the CV model. The cumulative distribution functions (CDFs) of multilateration [31], EKF, and the proposed algorithm are shown in Fig. 7. As shown in this figure, the proposed algorithm demonstrated better localization performance in both experiments. In the case of circular flight,
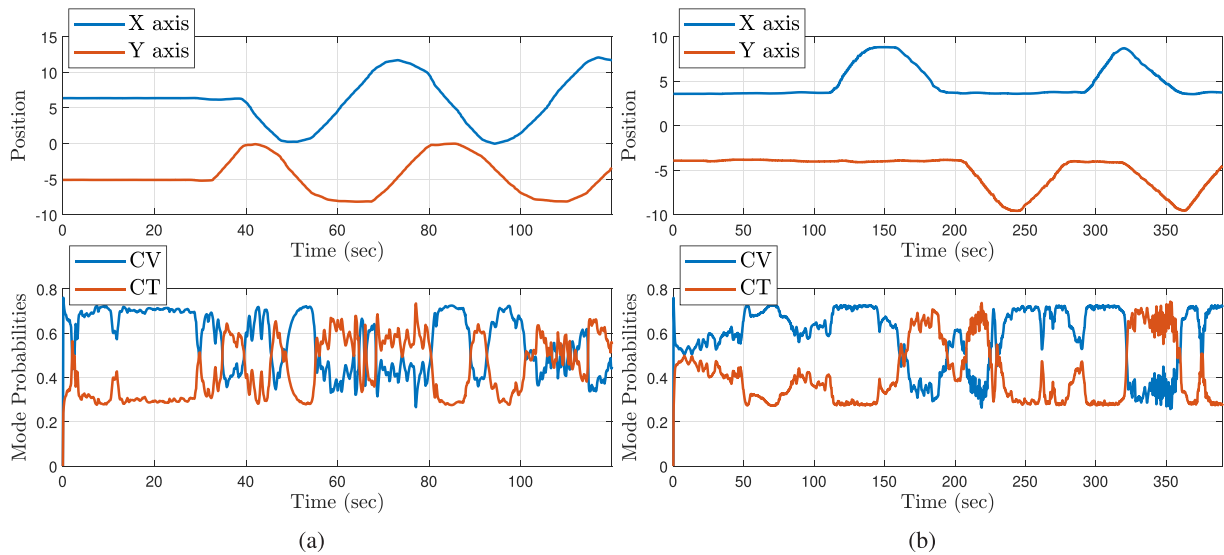
FIGURE 8. Mode probabilities of the proposed algorithm during (a) circular and (b) triangular motions.
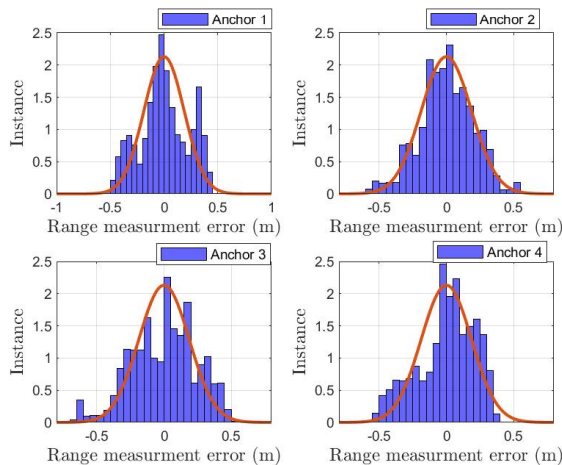

FIGURE 9. Error distribution of UWB range measurements for four UWB anchors.

multilateration performed better than EKF, but in the case of triangular flight, the opposite result was obtained.

Fig. 7 illustrates the subfilter modes (CV and CT) of the proposed IMM algorithm for the *x*- and *y*-axis positions of the UAV over time. As shown in this figure, when trajectory curvature occurs, the mode value of the CT model increases, while the mode value of the CV model decreases. In contrast, in the case of a trajectory segment with constant-velocity linear motion, the CV mode value is generally larger than the CT mode value.

The proposed IMM algorithm assumes that the UWB sensor noise follows a Gaussian distribution with an average value of 0. To verify the validity of this assumption, the error distribution of the UWB measurement values was analyzed and compared with a Gaussian distribution. As shown in the corresponding figure, it was confirmed that for each of the four sensors, the noise approximated a Gaussian distribution. Based on this error distribution analysis, the measured noise

covariance $\mathbf{R}_k$ was selected, and the proposed algorithm was executed.

VI. CONCLUSION

In this paper, we propose a system that allows the UWB range coverage to be freely modified by a single GCS controlling multiple UAVs equipped with UWB anchors. In addition, the heading information from an AHRS and UWB measurement values are combined to improve the localization accuracy compared to existing algorithms by means of a constrained IMM filter. This algorithm is easy and convenient to apply and requires only a small amount of calculation because only the heading information from the AHRS is required regardless of the type of UAV. Therefore, this system enables accurate location estimation while using UAVs to modify the UWB coverage area in an environment where GPS signal acquisition is difficult.

However, the IMM filter-based UWB positioning system has a delay due to the nature of the soft handoff algorithm that interacts between the subfilters of the IMM. As a future work, we will utilize deep learning-based mode estimation to reduce the interaction delay between sub-filters.

REFERENCES

[1] Y. Xu, Y. S. Shmaliy, C. K. Ahn, T. Shen, and Y. Zhuang, "Tightly coupled integration of INS and UWB using fixed-lag extended UFIR smoothing for quadrotor localization," *IEEE Internet Things J.*, vol. 8, no. 3, pp. 1716–1727, Feb. 2021.

[2] R. Mahony and V. Kumar, "Aerial robotics and the quadrotor," *IEEE Robot. Autom. Mag.*, vol. 19, no. 3, p. 19, Sep. 2012.

[3] T. Tomic, K. Schmid, P. Lutz, A. Domel, M. Kassecker, E. Mair, I. L. Grixa, F. Ruess, M. Suppa, and D. Burschka, "Toward a fully autonomous UAV: Research platform for indoor and outdoor urban search and rescue," *IEEE Robot. Autom. Mag.*, vol. 19, no. 3, pp. 46–56, Sep. 2012.

[4] J. A. Paredes, F. J. Álvarez, M. Hansard, and K. Z. Rajab, "A Gaussian process model for UAV localization using millimetre wave radar," *Expert Syst. Appl.*, vol. 185, Dec. 2021, Art. no. 115563.

[5] Y. Yang, X. Liu, W. Zhang, X. Liu, and Y. Guo, "Multilayer low-cost sensor local-global filtering fusion integrated navigation of small UAV," *IEEE Sensors J.*, early access, Jun. 23, 2021, doi: 10.1109/JSEN.2021.3091687.

[6] S. Moon, W. Youn, and H. Bang, "Novel deep-learning-aided multimodal target tracking," *IEEE Sensors J.*, vol. 21, no. 18, pp. 20730–20739, Sep. 2021.

[7] W. Youn, H. Ko, H. Choi, I. Choi, J.-H. Baek, and H. Myung, "Collision-free autonomous navigation of a small UAV using low-cost sensors in GPS-denied environments," *Int. J. Control, Autom. Syst.*, vol. 19, no. 2, pp. 953–968, Feb. 2021.

[8] A. R. Lopez, "GPS landing system reference antenna," *IEEE Antennas Propag. Mag.*, vol. 52, no. 1, pp. 104–113, Feb. 2010.

[9] M. Zhou, Y. Wang, Y. Liu, and Z. Tian, "An information-theoretic view of WLAN localization error bound in GPS-denied environment," *IEEE Trans. Veh. Technol.*, vol. 68, no. 4, pp. 4089–4093, Apr. 2019.

[10] B. Yang, L. Guo, R. Guo, M. Zhao, and T. Zhao, "A novel trilateration algorithm for RSSI-based indoor localization," *IEEE Sensors J.*, vol. 20, no. 14, pp. 8164–8172, Jul. 2020.

[11] F. Jiang, F. Pourpanah, and Q. Hao, "Design, implementation, and evaluation of a neural-network-based quadcopter UAV system," *IEEE Trans. Ind. Electron.*, vol. 67, no. 3, pp. 2076–2085, Mar. 2020.

[12] A. B. Junaid, Y. Lee, and Y. Kim, "Design and implementation of autonomous wireless charging station for rotary-wing UAVs," *Aerosp. Sci. Technol.*, vol. 54, pp. 253–266, Jul. 2016.

[13] M. N. Elya, S. B. M. Noor, A. R. R. Zafira, and S. Azrad, "Implementation of extended high-gain observer in low-cost optitrack motion tracking system for UAV control," in *Proc. IEEE 15th Student Conf. Res. Develop. (SCOReD)*, Dec. 2017, pp. 29–34.

[14] R. Mur-Artal, J. M. M. Montiel, and J. D. Tardós, "ORB-SLAM: A versatile and accurate monocular SLAM system," *IEEE Trans. Robot.*, vol. 31, no. 5, pp. 1147–1163, Oct. 2015.

[15] C. Forster, Z. Zhang, M. Gassner, M. Werlberger, and D. Scaramuzza, "SVO: Semidirect visual odometry for monocular and multicamera systems," *IEEE Trans. Robot.*, vol. 33, no. 2, pp. 249–265, Apr. 2017.

[16] R. Wang, M. Schworer, and D. Cremers, "Stereo DSO: Large-scale direct sparse visual odometry with stereo cameras," in *Proc. IEEE Int. Conf. Comput. Vis. (ICCV)*, Oct. 2017, pp. 3903–3911.

[17] K. Guo, X. Li, and L. Xie, "Ultra-wideband and odometry-based cooperative relative localization with application to multi-UAV formation control," *IEEE Trans. Cybern.*, vol. 50, no. 6, pp. 2590–2603, Jun. 2020.

[18] M. M. Sani, R. Chowdhury, and R. K. Chaudhary, "An ultra-wideband rectangular dielectric resonator antenna with MIMO configuration," *IEEE Access*, vol. 8, pp. 139658–139669, 2020.

[19] Y. Meng, W. Wang, H. Han, and J. Ban, "A visual/inertial integrated landing guidance method for UAV landing on the ship," *Aerosp. Sci. Technol.*, vol. 85, pp. 474–480, Feb. 2019.

[20] W. You, F. Li, L. Liao, and M. Huang, "Data fusion of UWB and IMU based on unscented Kalman filter for indoor localization of quadrotor UAV," *IEEE Access*, vol. 8, pp. 64971–64981, 2020.

[21] H. Chen, W. Xian-Bo, J. Liu, J. Wang, and W. Ye, "Collaborative multiple UAVs navigation with GPS/INS/UWB jammers using sigma point belief propagation," *IEEE Access*, vol. 8, pp. 193695–193707, 2020.

[22] W. Wang, D. Marelli, and M. Fu, "Multiple-vehicle localization using maximum likelihood Kalman filtering and ultra-wideband signals," *IEEE Sensors J.*, vol. 21, no. 4, pp. 4949–4956, Feb. 2021.

[23] Y. Xu, Y. S. Shmaliy, T. Shen, D. Chen, M. Sun, and Y. Zhuang, "INS/UWB-based quadrotor localization under colored measurement noise," *IEEE Sensors J.*, vol. 21, no. 5, pp. 6384–6392, Mar. 2021.

[24] Y. Zhang, X. Tan, and C. Zhao, "UWB/INS integrated pedestrian positioning for robust indoor environments," *IEEE Sensors J.*, vol. 20, no. 23, pp. 14401–14409, Dec. 2020.

[25] C. Wang, A. Xu, J. Kuang, X. Sui, Y. Hao, and X. Niu, "A high-accuracy indoor localization system and applications based on tightly coupled UWB/INS/Floor map integration," *IEEE Sensors J.*, vol. 21, no. 16, pp. 18166–18177, Aug. 2021.

[26] S. Moon, D. Lee, D. Lee, D. Kim, and H. Bang, "Energy-efficient swarming flight formation transitions using the improved fair Hungarian algorithm," *Sensors*, vol. 21, no. 4, p. 1260, Feb. 2021, doi: 10.3390/s21041260. [Online]. Available: https://www.mdpi.com/1424-8220/21/4/1260

[27] L. Meier, P. Tanskanen, F. Fraundorfer, and M. Pollefeys, "PIXHAWK: A system for autonomous flight using onboard computer vision," in *Proc. IEEE Int. Conf. Robot. Autom.*, May 2011, pp. 2992–2997.

[28] W. Youn and H. Myung, "Robust interacting multiple model with modeling uncertainties for maneuvering target tracking," *IEEE Access*, vol. 7, pp. 65427–65443, 2019.

[29] Y. Bar-Shalom, X. R. Li, and T. Kirubarajan, *Estimation With Applications to Tracking and Navigation: Theory Algorithms and Software*. Hoboken, NJ, USA: Wiley, 2004.

[30] H. Zhou, Z. Yao, and M. Lu, "UWB/Lidar coordinate matching method with anti-degeneration capability," *IEEE Sensors J.*, vol. 21, no. 3, pp. 3344–3352, Feb. 2021.

[31] A. Norrdine, "An algebraic solution to the multilateration problem," in *Proc. 15th Int. Conf. Indoor Positioning Indoor Navigat.*, Sydney, NSW, Australia, vol. 1315, 2012, pp. 1–4.

SUNGTAE MOON received the B.S. degree from Chonnam National University, Gwangju, South Korea, in 2005, the M.S. degree from the Gwangju Institute of Science and Technology (GIST), Gwangju, in 2007, and the Ph.D. degree in aeronautical engineering from KAIST, in 2021. From 2007 to 2010, he was with the Agency for Defense Development (ADD), where he developed a mission computer for aircraft. From 2011 to 2012, he was with the National Security Research Institute (NSRI) and worked in the area of security in embedded systems. Since 2012, he has been a Senior Researcher with the Artificial Intelligence Research Division of the Korea Aerospace Research Institute (KARI). Since 2022, he has been with the Korea University of Technology and Education (KOREATECH), Cheonan-si, South Korea, where he is currently an Assistant Professor with the School of Computer Science and Engineering. His current research interests include swarming flight systems, navigation algorithm, and object detection based on deep learning.

WONKEUN YOUN received the B.S. degree from Handong Global University, Pohang-si, South Korea, in 2008, and the M.S. degree in mechanical engineering and the Ph.D. degree in robotics from the Korea Advanced Institute of Science and Technology (KAIST), Daejeon, South Korea, in 2010 and 2020, respectively. From 2011 to 2021, he was a Senior Researcher with the Unmanned Aircraft System Research Division, Korea Aerospace Research Institute (KARI). Since 2021, he has been an Assistant Professor with Chungnam National University. His current research interests include multisensor fusion, Bayesian estimation theory, multimodal target tracking, and GPS/INS-based navigation.

• • •